Impact of inorganic waste fines on structure of mullite microspheres by reaction sintering

Impact of inorganic waste fines on structure of mullite microspheres by reaction sintering

J. Pype[a,b], B. Michielsen[a*], S. Mullens[a], V. Meynen[b]

[a] Sustainable Materials Management, Flemish Institute for Technological Research NV – VITO NV, Boeretang 200, 2400 Mol, Belgium

[b] Laboratory of Adsorption and Catalysis (LADCA), Department of Chemistry, University of Antwerp, CDE, Universiteitsplein 1, 2610 Wilrijk, Belgium

* Corresponding author: bart.michielsen@vito.be

Abstract

The impact of waste composition and morphology on the properties of the mullite microstructure were studied by reaction sintering two types of siliceous waste powders with calcined alum sludge. Stoichiometric mixtures of fly ash or rice husk ash with the alum sludge were shaped into mullite microspheres by droplet coagulation. The mullitization reaction was followed by HT-XRD with a distinct difference in onset temperature. The specific powder composition of fly ash (presence of primary mullite) shifted the onset temperature to higher values as compared to the rice husk ash mixture. After sintering at 1600 °C, the mullitization reaction resulted in the same yield for both samples. Although the mullite content in the microspheres was equal, distinct differences on the microstructure could be observed. Reaction sintering of the fly ash mixture resulted in lower total porosity with smaller pore sizes.

Keywords

Mullite, Rice husk ash, Fly ash, Alum sludge, Microspheres

1. Introduction

During the last decades, mullite has received significant attention as a potential material for various applications. Its attractive properties such as good chemical stability, low thermal expansion coefficient (4.5 x10-6 °C-1), and thermal shock resistance enables the use of mullite as catalyst support in high temperature combustion processes[1][2]. Shaping the catalyst support in the proper shape and size is key to unlock its excellent performance in processes. The choice of the size, shape and porous architecture are mainly driven by the type of reactor, all with their own demands concerning the support properties[3]. For example, fluidized bed reactors require spherical supports with a narrow size and shape distribution to prevent catalyst loss due to mechanical attrition[4]. One of the known methodologies to achieve such requirements in shaping ceramic microspheres with controlled properties is droplet coagulation [5][6][7]. Microspheres are shaped by the ionotropic gelation of sodium alginate with a multivalent cation, offering a wide range of process parameters (e.g. concentrations, alginate and cation type and powder properties) to control the microsphere properties.

Different types of synthesis (chemical, fused, reaction sintered) to prepare mullite were demonstrated in previous studies, varying in reaction mechanism and precursors[2]. Chemical mullite materials are prepared by heat treatment of organic and/or inorganic precursors (e.g. tetraethoxysilane and aluminum sec-butylate) with consequently a low mullitization temperature (below 1200 °C)[8]. Fused mullite is obtained by melting alumina and silica above 2000 °C, enabling the preparation of translucent materials[9]. Rodrigo et al. studied the reaction sintering of fine-grained powders to obtain dense mullite structures. Firing powder mixtures of silica and alumina at 1600 °C resulted in mullite with high purity[10]. During the past years, a wide range of starting materials was used to shape mullite materials, indicating also the potential use of inorganic waste powders as raw material[11],[12]. Often the mullitization reaction is enabled by the incorporation of an inorganic waste powder in a primary material as for example fly ash in bauxite alumina[13]. In this way, the cost effectiveness of the mullite preparation can be controlled. Vieira et. al. prepared mullite by smart mixing of alum sludge (anodization process) and slate waste resulting in mullite materials[14]. However, the impact of the properties of the waste resources on the mullite preparation and sintered materials were not elucidated. Nevertheless, the variations in chemical composition, morphology and waste impurities (e.g. TiO2, Fe2O3) can have a promoting or inhibiting effect on the sintering of mullite materials, with consequently an impact on the obtained porosity and microstructure[15][16].

This work stipulates the added value of mixing different fine-grained waste materials without the use of primary materials, in order to tune mullite materials with different properties and microstructures. In this study, calcined alum sludge is used as a substitute for commercial alumina. Alum sludge is generated as a byproduct of waste water treatment. It originates from the addition of an aluminum salt (e.g. $AlCl_3$) to polluted surface water, enabling the coagulation of natural organic matter (NOM) into sludge[17]. This alum sludge contains colloidal aluminum hydroxides (36 wt% aluminum content) in the presence of process additives (e.g. flocculant) and additional impurities (e.g. $Al_2(SO_4)_3$, calcium)[18]. Previous work specified the need of pre-processing (calcination and washing), enabling the shaping of alum sludge into microspheres by droplet coagulation[18]. As mullite microspheres are based on the stoichiometric mixture (3:2) of Al_2O_3 and SiO_2, silica rich waste powders were selected to add to the calcined alum sludge material. Both fly ash and rice husk ash are candidates as they contain high amounts of SiO_2 in their matrix [19][20]. Substantial amounts of fly ash (FA) are generated by coal firing for power generation. Additionally, the depletion of fossil fuels for the power generation has stimulated the utilisation of biomass as a source of fuel. Hence, this generates a new type of inorganic ash. Among the various biomass resources, rice husk is one of the key residues for energy production[21]. The combustion of the rice hulls, in order to acquire energy, leads to the production of rice husk ash (RHA). These two types of SiO_2 waste sources have been added to the alum sludge to investigate the ability to form mullite microspheres from 100% waste based resources as well as the consequences of the waste origin and composition on the microstructure of the mullite spheres.

The prime objective of this paper is to investigate the applicability of silica and alumina rich waste powders as precursors for the mullite preparation. Calcined alum sludge was mixed with two different silica waste fines (FA and RHA). Changes in mullitization reaction and mullite properties are expected originating from the differences in physical and chemical properties of the waste fines. Our aim is to study the extent of this impact of waste properties on the mullite preparation and consequently on the properties of the sintered microspheres. Furthermore, shaping microspheres by droplet coagulation incorporates a hetero-element (e.g. calcium) in the microstructure[6]. Hence, also the presence of the added calcium will be evaluated.

2. Materials and methods

2.1.Materials

Silpozz was supplied as rice husk ash (RHA) source (NK Enterprises, India). Fly ash (FA) was collected from the Tarong Power Station (Australia). Alum sludge (AS) was collected at the water treatment plant of "De Watergroep" (Kluizen, Belgium) and pre-processed as described in our previous paper[22]. Sodium alginate Br-W was provided by Brace GmBH (Alzenau, Germany). Additionally, calcium chloride (Sigma Aldrich, anhydrous powder ≥97 % pure), isopropyl alcohol (VWR, 98%) and RO water (< 5 µS/cm) were used.

2.2.Shaping microspheres

Prior to shaping the microspheres, a suspension containing 1 wt% sodium alginate and 30 wt% powder was prepared. Mixtures of the waste powders were made based on the chemical composition analyzed by XRF on the melt. The AS-FA (77.2% AS and 22.8% FA) and AS-RHA (83.7% AS and 16.3% RHA) suspensions were prepared by mixing stoichiometric amounts of respectively AS, FA and RHA with the sodium alginate solution in a planetary mixer. In addition, an AS suspension was prepared in order to distinguish the effect of the mullitization on the sintering process. The microspheres were shaped by gravitational droplet coagulation and denoted as AS/M, AS-FA/M and AS-RHA/M. During shaping, the suspension was pushed through a 600 µm nozzle (Nordson EFD) and droplets were generated by gravitational force. The droplets fell in a coagulation bath containing 4 wt% $CaCl_2$, in order to induce the ionotropic coagulation. After 24 hours, the wet microspheres were rinsed with tap and RO water to remove the excess of ions. Finally, the microspheres were washed with isopropyl alcohol to reduce capillary forces during drying. The microspheres were dried at 105 °C for 24 hours and sintered at varying temperatures between 1400 to 1600 °C with a heating rate of 2 °C/min under ambient air and pressure.

2.3.Characterization techniques

The chemical composition of the initial waste powders was examined by X-ray fluorescence (XRF) (HE XEPOS, Spectro Analytical Systems, Kleve, Germany). The powders were calcined at 1000 °C for 4 hours in a muffle furnace prior to mixing in a platinum crucible with 100% $Li_2B_4O_7$ flux in a flux:sample ratio of 10:1. The fusion of the sample was performed in an automatic fusion system (XrFuse 2, XRF Scientific, Brussels, Belgium), in which the sample was fused at 1250°C during 11 minutes. An NH_4I tablet was added as release agent prior to pouring the fused sample in the pre-

heated mold. Quantification of the elements was performed using a precalibrated software package for the quantitative analysis of geological fused bead materials.

The starting powders and sintered microspheres were characterized using X-ray diffraction (XRD) analysis (X'Pert Pro MPD diffractometer, PANalytical) with filtered Cu K_α irradiation. The analysis was executed in the 2θ mode using a bracket sample holder with scanning speed of 0.04°/4s continuous mode. The sintered microspheres were milled prior to the analysis.

The crystal phase changes in function of the temperature of thermal treatment were identified by high temperature X-ray diffraction analysis (HT-XRD, X'Pert Empyrean, PANalytical) with a high temperature chamber HTK 16 (Anton Paar) and applying Co K_α irradiation. The milled microspheres were placed on the platina sample holder and heated to 800 °C (10 °C/min). The sample was further heated to 1400 °C at a constant heating rate (10 °C/min) and XRD patterns were collected in steps of 100 °C. The measurements were conducted in dry air (50 ml/min).

Thermogravimetric analysis (TGA) was carried out using a STA 449 F3 Jupiter (Netzsch, Germany) in dry air (50 ml/min). The microspheres were analyzed from room temperature to 1500 °C (10 °C/min). The TGA device was coupled online with a quadrupole mass spectrometer TGA/STA-QMS 403 D Aëolos (Netzsch, Germany) with a heated capillary (200 °C).

To study the sintering behavior, pellets of crushed microspheres were analysed using a DIL 402 C dilatometer (Netzsch, Germany) in dry air (70 ml/min). The pellets were measured between room temperature and 1600 °C (10 °C/min).

The shape of the sintered microspheres was determined by optical microscopy using a Zeiss Discovery V12 stereomicroscope, equipped with a Plan Apo S 1.0 w FWD 60 mm objective. An Axiovision MRc digital camera connected to the microscope was used to generate images of the microspheres. Axiovision Rel. 4.8 software was employed to perform image processing as explained in earlier work[6].

The cross-section of the microspheres was investigated using a cold field emission scanning electron microscope (FEGSEM) of the type Nova Nano SEM 450 (FEI, USA) at 20 kV. The microspheres were encapsulated in epoxy resin, cut and polished prior to the analysis. Element mapping was performed by a Bruker XFlash Detector 5030 and a Bruker QUANTAX-200 EDS system. The total porosity was calculated on the cross-section using ImageJ. The outer surface of the microspheres was characterized at 5 kV.

The specific pore volume and pore size distribution was measured with mercury intrusion porosimetry (Pascal 140-240 series, Thermo Electron Corporation). The pore size was calculated using a surface tension of 480 Dynes/cm and a contact angle of 140°.

The side crushing strength (SCS) test on an Instron 5582 Universal testing machine was used to estimate the crushing strength of the sintered microspheres, following Couroyer et al.[23]. Ten spheres were crushed to calculate the average strength on a single shaped microsphere.

3. Results and discussion

3.1. Characterization of starting materials

Component		*RHA*	*FA*	*AS*
SiO_2	%	92	70	9.8
Al_2O_3	%	-	24	69
K_2O	%	1.2	0.6	-
CaO	%	0.9	-	1.5
TiO_2	%	-	1.4	-
MnO	%	0.1	-	0.1
Fe_2O_3	%	0.4	2.0	-

3.2.

Table 1: Chemical composition of RHA, FA and AS powder determined by XRF on the melt

The fine-grained waste powders contained primarily different ratios of Al_2O_3 and SiO_2 in combination with some impurities, as shown in Table 1. The RHA powder consists of mainly SiO_2 (92 wt%). The XRD pattern (Figure 1) revealed a combination of quartz and cristobalite, originating from the high temperature applied in the combustion process of the RHA powder[24]. The broad diffraction peak between 10° and 40° indicates the additional presence of amorphous silicate glassy phase. On the other hand, the combustion of siliceous coal resulted in FA with 70 wt% SiO_2 and 24wt% Al_2O_3 in combination with K_2O, TiO_2 and Fe_2O_3 impurities. The XRD pattern of FA represents the combination of amorphous and crystalline phases, with the major crystalline phases: mullite ($3Al_2O_3.2SiO_2$) and quartz. The mullite belongs to the primary mullite formed out of the aluminosilicate clays during the coal combustion process itself[25]. The amorphous silicate phase between 10° and 40° is correlated to the rapid cooling in the coal combustion process[13]. The alum sludge (AS) is mainly composed of

aluminum components (69 wt% Al_2O_3) in combination with a small amount of SiO_2 (9.8 wt%) and CaO (1.5wt%). The XRD pattern of the AS powder reveals the presence of amorphous phases with indications of quartz and δ-Al_2O_3. Based on the XRF elemental composition, the mass ratio of AS to FA or RHA was calculated to obtain a 3:2 ratio of Al_2O_3:SiO_2 in the AS-FA and AS-RHA powder. Due to differences in the silica to alumina ratio of the FA and RHA, different ratios were used in the AS-FA and AS-RHA mixtures: AS-FA contains 23 wt% FA in combination with the alum sludge, whereas the AS-RHA contains 16 wt% of RHA.

Figure 1

3.2.Shaping microspheres

The AS, AS-FA and AS-RHA powders were mixed with sodium alginate to prepare the ceramic suspension. Rheological analysis of these suspensions revealed shear thinning behavior at increasing shear rates. High agitating forces caused the disintegration of the rigid structure by reducing the particle-particle interactions. This shear thinning is independent of the powder morphology or composition as shown in Figure 2. However, monodisperse droplets could be shaped without any impact of this shear thinning behavior[26] and solidified in a $CaCl_2$ coagulation bath. In the coagulation process, the sodium ions are exchanged with the divalent calcium ions causing the ionotropic gelation to solidify the droplets into gelled microspheres[7]. Subsequently, after shaping, the microspheres were rinsed and dried prior to further thermal processing.

Figure 2

3.3.Thermal behavior of the AS, AS-FA and AS-RHA microspheres

The dried microspheres are calcined to remove the organic matter of both the original waste powders and the calcium alginate of the binder system[22]. The calcination is simulated in the TGA-MS analysis. The weight loss (TG) and derivative of the weight loss (DTG) profiles in correlation to the mass spectra are shown in Figure 3 and Figure 4.

Figure 3

Figure 4

The weight loss in the temperature range from 30 to 200 °C is correlated to the evolution of H_2O (m/z=18) in the MS data. In this region, the loss of physisorbed water on the microspheres and

decomposition of $Al(OH)_3$ of the alum sludge occurs. The decomposition of calcium alginate is characterized by a two-step process, as indicated in earlier work[6]. The different steps are difficult to distinguish in the broad DTG profile, however identification of the weight losses can be made based on the MS data. The oxidation of calcium alginate occurs simultaneously with the further decomposition of $Al(OH)_3$ between 200 and 400 °C. The H_2O and CO_2 (m/z= 44) signals in the MS data confirm the oxidation reaction, where the $Al(OH)_3$ only generates H_2O. Subsequently, the decarboxylation occurs between 400 and 600 °C with the evolution of CO_2. The temperature range of the decarboxylation reaction is influenced by the type of silicate (FA or RHA) added and the different impurities present in the waste powders. An additional step in the AS-RHA/M sample (DTG max at 450 °C) can be correlated to oxidation of carboneous material in the RHA powder itself (Figure S1) [27]. The CO_2 profile of AS-FA/M indicates an additional decomposition between 500 and 800 °C, correlated to the carbon oxidation of the carbonaceous material present in the FA waste stream (Figure S1) [28]. The DTG profiles of all compositions indicate a maximum at 920 °C that can be correlated to CO_2 and SO_2. Two phenomena can be distinguished at this temperature. The CO_2 signal is associated with the decomposition of $CaCO_3$ in CaO, which is an intermediate product of the calcination of calcium alginate[29]. Additionally the SO_2 is in correlation with the decomposition of $Al_2(SO_4)_3$ that originates from the alum sludge powder[22]. The final weight loss can be observed in the temperature range of 1000 °C to 1500 °C, contributed by the decomposition of $CaSO_4$ into CaO and SO_2. The residual CaO will affect the further sintering of the microspheres as indicated in earlier work[6][22].

In order to distinguish the different crystal phases formed during the thermal processing of the microspheres, HT-XRD was performed on crushed microspheres (Figure 5). All HT-XRD diffractograms indicated platinum (Pt) peaks (46° and 54°), originating from the substrate on which the samples were put for analysis. Increasing the temperature caused widening of the peaks.

Figure 5

The mullite preparation by reaction sintering the waste mixtures was determined in the HT-XRD profiles in correlation to the waste composition. Despite the fact that no silica phase is mixed in AS/M microspheres, small amounts of mullite are formed at 1200 °C. The alum sludge itself contains small amounts of silica in the alumina matrix, resulting in reaction sintered mullite. Mixing silica rich RHA in the alum sludge (AS-RHA/M) results in mullite formation with its first signals at 900 °C (32° 2θ). The mullite signals further increase in intensity at elevated temperatures. In contrast to the AS-

RHA/M, the determination of the mullite onset temperature was not possible in the AS-FA/M due to the composition of the FA powder. Mullite signals were already present at 800 °C due to the presence of primary mullite. Nevertheless, the reaction sintering of alum sludge with fly ash resulted in additional mullite formation, starting at 1300 °C, as observed by the increased intensity of the mullite signals. Besides the presence of mullite, other polymorphs crystallize during the heat treatment, such as α-alumina. The α-Al_2O_3 becomes visible at 1200 °C in the AS/M sample, whereas the onset temperature increased to 1300 °C in the mixed samples (AS-FA/M and AS-RHA/M). As indicated in the TGA-MS analyses, CaO is the residual product of the calcium alginate decomposition. This residual CaO leads to the formation of calcium aluminium silicate (CA)[30]. A first CA peak was observed at 1100 °C (25°) in the AS-RHA/M sample while the onset in AS/M and AS-FA/M was shifted to 1300°C. This temperature difference is due to a promoting effect of the RHA waste matrix. Furthermore, additional silica phases were observed in AS-FA/M (cristobalite and quartz) and AS-RHA/M (a minor amount of cristobalite) due to incomplete mullitization. The initial quartz of raw FA powder partially transforms in cristobalite at high temperature[11]. As visible in the HT-XRD diffractograms, the mullite formation is influenced by the chemical composition of the waste fines. These results show that the mullite onset temperature and the polymorph mixture during sintering differ for the AS-FA/M and AS-RHA/M microspheres.

To further explore, the sintering onset temperatures and shrinkage behaviors are determined by dilatometry analyses in correlation to their polymorph transformation as indicated in the HT-XRD analyses. Figure 6 shows the dL/L_o and dL/dt curves of the AS/M, AS-FA/M and AS-RHA/M samples. The dilatometry data are summarized in Table 2.

Figure 6

	Onset 1 (°C)	*dL/dt (°C)*	*Onset 2 (°C)*	*dL/dt (°C)*	*Onset 3 (°C)*	*dL/dt (°C)*	*dL/Lo (%)*
AS/M	827	952	1050	1215	1320	1546	-22
AS-FA/M	820	948	1045	1210	1301	1407	-13
AS-RHA/M	830	943	995	1202	1292	1369	-14

Table 2: Overview of the dilatometry data. Total shrinkage (dL/Lo) obtained in the temperature range from 800 to 1600 °C.

The sintering of all samples occurs in different steps, depending on their composition (Figure 6 and Table 2). The first broad shrinkage of AS/M is characterized by a dL/dt maximum at 952 °C, which could be correlated to the decomposition of Al2SO4 into alumina and SO2 gas with consequently a shrinkage (2 %) of the sample as a result. The decomposition of Al2SO4 is in correlation to the weight loss and gaseous evolution in the TGA-MS data (Figure 3 and Figure 4), with some difference in amount of Al2SO4 between the AS/M and the composite mixtures. The total sintering shrinkage was calculated from 800 to 1600 °C, in order to include the shrinkage induced by the Al2SO4 decomposition. In case of AS/M, the second stage starts at 1050 °C with its dL/dt maximum at 1215 °C. The sintering is temporarily inhibited above 1215 °C due to the release of SO2 gas caused by the decomposition of CaSO4[31]. The densification of AS/M restarted at 1320 °C, reaching its dL/dt maximum at 1546 °C with a total shrinkage of 22% in the sintering temperature range (800 to 1600 °C). The presence of CA, as indicated in HT-XRD, will enhance the sintering diffusion due to its liquid melt at 1553 °C[32]. Sintering the AS-FA and AS-RHA microspheres followed a different shrinkage profile due to their unique composition. As indicated in the literature, the densification of mullite can be influenced by the presence of various impurities as present in the raw fly ash and rice husk ash[33][34]. The sintering onset temperature of the AS-RHA/M pellet is observed at 995 °C with 7 % shrinkage. Similar to AS/M, at 1202 °C the densification was inhibited. At this temperature two processes are occurring. The first is analog to the AS/M where the release of SO2 gas inhibited sintering. Secondly, the mullitization reaction could result in volume expansion hindering the densification of AS-RHA/M. Above 1292 °C, the densification continued with its dL/dt max at 1369 °C and a total shrinkage of 14 % at 1600 °C. Consequently, the AS-RHA/M microspheres shrink considerable less than the alum sludge spheres (22%) where no silica was added. The pellet of the AS-FA/M followed the same sintering steps as AS-RHA/M. However, the densification was delayed as indicated by the differences of the dL/dt maximum between AS-FA/M and AS-RHA/M. The differences in densification are in correlation to their differences in chemical composition and morphology (Table 1 and Figure S2). The AS-FA/M sample started to sinter at 1045 °C, indicating a delay in sintering onset temperature compared to the use of RHA as silica resource, which could be in correlation to the titanium present in the raw FA powder [16]. Analog to the AS-RHA/M sample, a plateau was reached above 1210 °C. Analog to the AS-RHA/M, SO2 gas was released at this temperature with the concomitant mullite formation as demonstrated by the HT-XRD (Figure 5). The densification process restarted at 1301 °C with a delay in dL/dt max (1407 °C) compared to the RHA addition but still prior to densification in the AS/M sample. The HT-XRD analysis revealed the residual

presence of quartz at this temperature, resulting in further polymorph transitions that might hamper the densification process. The maximum densification was reached at 1600 °C, with a total shrinkage of 13%. Accordingly, no significant impact of the waste properties on the total shrinkage of the mullite spheres could be observed.

The microspheres were sintered 1 hour at 1400, 1500 and 1600 °C to study the impact of the sintering on the mullitization and microstructural properties. Rietveld refinement on the XRD patterns of the sintered microspheres enabled the quantitative evaluation of the mullite formation (Figure 7 and Table 3).

Figure 7

Figure S3 shows the diffraction patterns of AS/M, AS-FA/M and AS-RHA/M in function of the sintering temperature with its corresponding phase quantification in Figure 7. The XRD pattern of AS/M revealed the presence of α-Al_2O_3 as the end product (95%) of the thermal conversion of the initial amorphous $Al(OH)_3$. The intensity of α-Al_2O_3 increased in function of the sintering temperature. In addition, a small amount of mullite (5%) is present formed out of the initial presence of silica in the alum sludge. Calcium is present in all the microspheres due to a twofold effect. Calcium is an impurity of the alum sludge, as indicated in the XRF data (Table 1) and in addition it is added to the microspheres by the ionotropic gelation of the sodium alginate in the coagulation bath. The calcium induced the formation of calcium aluminum silicate ($Ca(Al_2Si_2O_8)$) in the microspheres during sintering. The HT-XRD (Figure 5) revealed a slightly higher intensity of CA in AS-RHA/M at 1400 °C. However, after sintering 1 hour at 1400 °C no distinct difference in CA could be noticed between AS/M, AS-FA/M and AS-RHA/M (Figure 7). Therefore, it could be presumed that the kinetics of CA formation are influenced by the RHA impurities, as also the onset temperature was 200 °C lower as compared to AS/M and AS-FA/M. Due to the melting of $Ca(Al_2Si_2O_8)$ at 1553 °C[35], its peak intensity disappeared at 1600 °C. The liquid $Ca(Al_2Si_2O_8)$ phase has an influence on the sintering, as visible on the SEM-EDX analysis on the cross section of the microspheres (Figure 8) and described in detail in our previous work[22]. The XRD analyses on AS-FA/M and AS-RHA/M revealed the almost complete mullitization of the microspheres after sintering 1 hour at 1600 °C. Sintering the AS-FA/M resulted in 96% mullite with slight presence of alumina in the matrix. This is in agreement with the SEM-EDX data showing little alumina grains in a matrix containing aluminium, silicium and calcium. Consequently, the $Ca(Al_2Si_2O_8)$ phase was homogeneously spread. Similar to the AS-FA/M microspheres, 97% mullite was obtained after sintering AS-RHA/M for 1 hour at 1600 °C.

Consequently, no distinct effect of the waste properties (chemical composition or morphology) could be observed on mullite yield after sintering.

SEM analysis on the outer surface of the microspheres (Figure 9) revealed the unique needle-like microstructure of mullite in both the AS-FA/M and AS-RHA/M microspheres, in contrast to the AS/M sample. The network of needle-like grains will strengthen the microspheres at high temperatures, as for example in thermal combustion processes[36]. In addition, the SEM analyses shown in Figure 8 and 9, revealed a difference in porosity between AS-FA/M and AS-RHA/M. Iron and alkali cations induce the formation of a liquid phase, causing enhanced diffusion along the mullite grains with its impact on the porosity. Since the formation of this liquid phase is a function of the amount, type of impurity and homogeneity of its distribution , a variety of porous and microstructural properties can be obtained by smart mixing of siliceous and alumina waste fines.

Figure 8

Figure 9

Mercury intrusion porosimetry in function of the sintering temperature was performed to quantify the differences in porosity. Figure 10 reveals the impact of the sinter profile on the open pore volume, with a shift to lower values at elevated temperatures. The AS/M sample becomes almost completely dense at 1600 °C while the two other materials with a high mullite fraction remain porous. This difference in densification was also visible in the dilatometer analysis, resulting in less total shrinkage. No distinct difference in open pore volume could be noticed for the AS-FA/M and AS-RHA/M after sintering at 1600 °C, however apparent differences in pore sizes could be observed. The average pore size of the AS-FA/M microspheres after sintering at 1600 °C is 3 µm as compared to 9 µm for the AS-RHA/M sample. In addition, the total porosity was quantified by segmentation of the SEM images of the microsphere cross sections (Figure S4). Distinct differences can be observed between AS-FA/M and AS-RHA/M (Table 3). 32% residual porosity was obtained after sintering the AS-FA/M in contrast to the 40% porosity in the AS-RHA/M sample. Although, the open pore volume of both samples was the same at 1600 °C, higher total porosity could be observed for the AS-RHA/M. This difference could be explained by the presence of some closed porosity in the AS-RHA/M spheres. As a result of the residual porosity, the mechanical strength of the mullite spheres is lower as compared to the alum sludge spheres (Figure S4). A minor difference could be observed between AS-FA/M and AS-RHA/M, which is in correlation to the variation in powder packing and total porosity. The microstructural variations of AS-FA/M and AS-RHA/M stipulate the consequences of the initial

waste properties on the mullitization. Therefore, one can think of further adjusting the materials properties by pre-processing (e.g. leaching, size reduction) of the waste fines. Furthermore, the versatile use of droplet coagulation (e.g. different coagulation precursors that alter the chemical composition of the spheres or changes in alginate/powder content etc.) combined with controllability of the thermal post-processing, provides additional flexibility of shaping mullite microspheres with a unique microstructure and porosity.

Figure 10

	Al_2O_3(%)*	*$3Al_2O_3.2SiO_2$*(%)*	*Porosity (%)*	*Crushing strength (MPa)*
AS/M	95	5	3.9 ± 0.7	185 ± 57
AS-FA/M	4	96	32 ± 1	32 ± 6
AS-RHA/M	3	97	40 ± 1	24. 3

Table 3: Overview of the microsphere characteristics after sintering 1 hour at 1600 °C (Rietveld refinement)*

4. Conclusion

Mixtures of fly ash and rice husk ash with calcined alum sludge were used to shape mullite microspheres. The effect of the mullitization on the thermal post processing was studied. Shaping mullite microspheres could be achieved without any impact of the waste composition. In contrast to the shaping step, the thermal post-processing step was influenced by the morphology and chemical composition of the waste fines. TGA-MS analyses indicated calcination profiles unique to the decomposition of the waste impurities, such as the oxidation of carboneous materials of the fly ash and rice husk ash at different temperatures. The onset temperature of the mullitization reaction was determined to be 900 °C in the AS-RHA/M. HT-XRD indicated that the onset temperature shifted to a higher temperature (1300 °C) in the AS-FA/M microspheres where primary mullite of the fly ash was present. Moreover, variations in polymorph transitions in the mullite microspheres could be observed. Although, the total shrinkage was equal for both mullite microspheres, different shrinkage profiles could be observed.

Rietveld refinement on the sintered microspheres (1600 °C) revealed high mullite yield (> 95%) for both mixtures. SEM-EDX showed the presence of small fractions of α-Al2O3 and amorphous Ca(Al2Si2O8) homogeneously spread between the mullite. Although the mullitization in both AS-FA/M and AS-RHA/M resulted in the same yield, distinct differences on the microstructures could be observed. The initial impurities and morphology of the fly ash and rice husk ash had a distinct impact on the pore size and total porosity. The mullitization and sintering of the fly ash and alum sludge mixture (AS-FA/M) resulted in lower total porosity (32 %) with smaller pore sizes (3 μm) than the AS-RHA/M materials. Hence, the impact of the waste composition on microstructure and porous properties has been stipulated for the shaping of mullite microspheres by smart mixing of waste fines.

Acknowledgement

This work was supported by the Agency for Innovation by Science and Technology in Flanders (IWT-131229), which granted J. Pype her PhD scholarship. The authors are very grateful to 'De Watergroep', Jef Bergmans and Ruben Snellings for supplying the alum sludge and fly ash. The technical staff of VITO is gratefully acknowledged for the support on the analyses of the materials, especially M. Mertens (XRD/HT-XRD), R. Kemps (SEM-EDX), and A. De Wilde (TGA-MS and Hg porosimetry).

Supporting information

Thermogravimetric analyses on rice husk ash (RHA), fly ash (FA) and alum sludge (AS-C). Particle size and shape distribution of RHA, FA and AS-C. XRD patterns of AS/M, AS-FA/M and AS-RHA/M in function of sintering temperature. Optical microscopy of sintered microspheres in correlation to the SEM images on their cross section. Crushing strength of the microspheres in function of sintering temperature.

References

[1] M.F.M. Zwinkels, S.G. Jaras, P.G. Menon, T.A. Griffin, Catalysis Reviews : Science and Engineering Catalytic Materials for High-Temperature Combustion, Catal. Rev. Sci. Eng. 35 (1993) 319–358. doi:10.1080/01614949308013910.

[2] H. Schneider, J. Schreuer, B. Hildmann, Structure and properties of mullite — A review, J. Eur. Ceram. Soc. 28 (2008) 329–344. doi:10.1016/j.jeurceramsoc.2007.03.017.

[3] M. Campanati, G. Fornasari, A. Vaccari, Fundamentals in the preparation of heterogeneous

catalysts, Catal. Today. 77 (2003) 299–314. doi:10.1016/S0920-5861(02)00375-9.

[4] Z.R. Ismagilov, R.A. Shkrabina, N.A. Koryabkina, New technology for production of spherical alumina supports for fluidized bed combustion, Catal. Today. 47 (1999) 51–71. doi:10.1016/S0920-5861(98)00283-1.

[5] C.J.E. Santos, T.-S. Wei, B. Cho, W.M. Kriven, A Forming Technique to Produce Spherical Ceramic Beads Using Sodium Alginate as a Precursor Binder Phase, J. Am. Ceram. Soc. 96 (2013) 3379–3388. doi:10.1111/jace.12584.

[6] J. Pype, B. Michielsen, E.M. Seftel, S. Mullens, V. Meynen, Development of alumina microspheres with controlled size and shape by vibrational droplet coagulation, J. Eur. Ceram. Soc. 37 (2017) 189–198. doi:10.1016/j.jeurceramsoc.2016.07.020.

[7] T.Y. Klein, L. Treccani, K. Rezwan, Ceramic Microbeads as Adsorbents for Purification Technologies with high specific surface area, adjustable pore size and morphology obtained by ionotropic gelation, J. Am. Ceram. Soc. 95 (2012) 907–914.

[8] H. Schneider, B. Saruhan, D. Voll, L. Merwin, A. Sebald, Mullite Precursor Phases, J. Eur. Ceram. Soc. 11 (1993) 87–94.

[9] H. Schneider, M. Schmucker, K.O. Ikeda, W.A. Kaysser, Optically Translucent Mullite Ceramics, J. Am. Ceram. Soc. 14 (1995) 2912–2914.

[10] P.D.D. Rodrigo, P. Boch, High Purity Mullite Ceramics by Reaction Sintering, Int. J. High Technol. Ceram. 1 (1985) 3–30.

[11] J.S. Jung, H.C. Park, R. Stevens, Mullite ceramics derived from coal fly ash, J. Mater. Sci. Lett. 20 (2001) 1089–1091. doi:10.1023/A:1010934728570.

[12] M.F. Serra, M.S. Conconi, M.R. Gauna, G. Suárez, E.F. Aglietti, N.M. Rendtorff, Mullite (3Al2O3·2SiO2) ceramics obtained by reaction sintering of rice husk ash and alumina, phase evolution, sintering and microstructure, J. Asian Ceram. Soc. 4 (2015) 1–7. doi:10.1016/j.jascer.2015.11.003.

[13] Y. Dong, X. Feng, X. Feng, Y. Ding, X. Liu, G. Meng, Preparation of low-cost mullite ceramics from natural bauxite and industrial waste fly ash, J. Alloys Compd. 460 (2008) 599–606. doi:10.1016/j.jallcom.2007.06.023.

[14] S.C. Vieira, A.S. Ramos, M.T. Vieira, Mullitization kinetics from silica- and alumina-rich wastes, Ceram. Int. 33 (2007) 59–66. doi:10.1016/j.ceramint.2005.07.015.

[15] Y. Dong, S. Hampshire, J. er Zhou, Z. Ji, J. Wang, G. Meng, Sintering and characterization of flyash-based mullite with MgO addition, J. Eur. Ceram. Soc. 31 (2011) 687–695. doi:10.1016/j.jeurceramsoc.2010.12.012.

[16] Y. Dong, S. Hampshire, J. er Zhou, B. Lin, Z. Ji, X. Zhang, G. Meng, Recycling of fly ash for

preparing porous mullite membrane supports with titania addition, J. Hazard. Mater. 180 (2010) 173–180. doi:10.1016/j.jhazmat.2010.04.010.

[17] C.S. Lee, J. Robinson, M.F. Chong, A review on application of flocculants in wastewater treatment, Process Saf. Environ. Prot. 2 (2014) 489–508. doi:10.1016/j.psep.2014.04.010.

[18] J. Pype, B. Michielsen, S. Mullens, V. Meynen, Versatile use of droplet coagulation: shaping fine-grained SiO2 and Al2O3 waste streams into monodisperse microspheres, Sustain. Mater. Technol. 14 (2017) 19–28. doi:10.1016/j.susmat.2017.11.001.

[19] R.S. Blissett, N.A. Rowson, A review of the multi-component utilisation of coal fly ash, Fuel. 97 (2012) 1–23.

[20] N. Soltani, A. Bahrami, M.I. Pech-Canul, L.A. Gonzalez, Review on the physicochemical treatments of rice husk for production of advanced materials, Chem. Eng. J. 264 (2015) 899–935. doi:10.1016/j.cej.2014.11.056.

[21] J.S. Lim, Z.A. Manan, S.R. Wan Alwi, H. Hashim, A review on utilisation of biomass from rice industry as a source of renewable energy, Renew. Sustain. Energy Rev. 16 (2012) 3084–3094. doi:10.1016/j.rser.2012.02.051.

[22] J. Pype, B. Michielsen, S. Mullens, V. Meynen, Versatile use of droplet coagulation: shaping fine-grained SiO2 and Al2O3 waste streams into monodisperse microspheres, Submitt. Waste Manag. (2017).

[23] C. Couroyer, M. Ghadiri, P. Laval, N. Brunard, F. Kolenda, Methodology for Investigating the Mechanical Strength of Reforming Catalyst Beads, Oil Gas Technol. 55 (2000) 67–85.

[24] Y. Shinohara, N. Kohyama, Quantitative analysis of tridymite and cristobalite crystallized in rice husk ash by heating., Ind. Health. 42 (2004) 277–285. doi:10.2486/indhealth.42.277.

[25] C.Y. Chen, G.S. Lan, W.H. Tuan, Microstructural evolution of mullite during the sintering of kaolin powder compacts, Ceram. Int. 26 (2000) 715–720. doi:10.1016/S0272-8842(00)00009-2.

[26] M.R. Davidson, J.J. Cooper-White, Pendant drop formation of shear-thinning and yield stress fluids, Appl. Math. Model. 30 (2006) 1392–1405. doi:10.1016/j.apm.2006.03.016.

[27] G.C. Cordeiro, R.D. Toledo Filho, E. de Moraes Rego Fairbairn, Use of ultrafine rice husk ash with high-carbon content as pozzolan in high performance concrete, Mater. Struct. 42 (2009) 983–992. doi:10.1617/s11527-008-9437-z.

[28] J. Payá, J. Monzó, M.. Borrachero, E. Perris, F. Amahjour, Thermogravimetric Methods for Determining Carbon Content in Fly Ashes, Cem. Concr. Res. 28 (1998) 675–686. doi:10.1016/S0008-8846(98)00030-1.

[29] T.R. Ingraham, P. Marier, Kinetic studies on the thermal decomposition of calcium carbonate,

Can. J. Chem. Eng. 41 (1963) 170–173.

[30] S. Kurama, E. Ozel, The influence of different CaO source in the production of anorthite ceramics, Ceram. Int. 35 (2009) 827–830. doi:10.1016/j.ceramint.2008.02.024.

[31] M.J. Ribeiro, D.U. Tulyaganov, J.M. Ferreira, J.A. Labrincha, Recycling of Al-rich industrial sludge in refractory ceramic pressed bodies, Ceram. Int. 28 (2002) 319–326. doi:10.1016/S0272-8842(01)00097-9.

[32] O.B. Fabrichnaya, I. Nerad, Thermodynamic properties of liquid phase in the CaO·SiO2–CaO·Al2O3·2SiO2–2CaO·Al2O3·SiO2 system, J. Eur. Ceram. Soc. 20 (2000) 505–515.

[33] M.L. Bouchetou, J.P. Ildefonse, J. Poirier, P. Daniellou, Mullite grown from fired andalusite grains: The role of impurities and of the high temperature liquid phase on the kinetics of mullitization and consequences on thermal shocks resistance, Ceram. Int. 31 (2005) 999–1005. doi:10.1016/j.ceramint.2004.10.015.

[34] G. Lecomte-Nana, J.P. Bonnet, N. Soro, Influence of iron on the occurrence of primary mullite in kaolin based materials: A semi-quantitative X-ray diffraction study, J. Eur. Ceram. Soc. 33 (2013) 669–677. doi:10.1016/j.jeurceramsoc.2012.10.033.

[35] J.R. Taylor, A.T. Dinsdale, Thermodynamic and phase diagram data for the CaO-SiO2 system, Calphad. 14 (1990) 71–88. doi:10.1016/0364-5916(90)90041-W.

[36] M.F.M. Zawrah, N.M. Khalil, Effect of mullite formation on properties of refractory castables, Ceram. Int. 27 (2001) 689–694. doi:10.1016/S0272-8842(01)00021-9.

Supplementary data

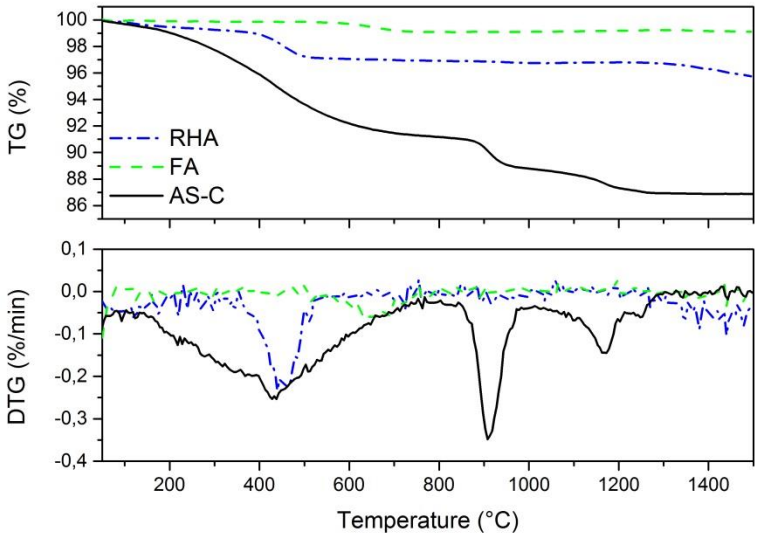

Figure S1: TG and DTG profiles of RHA, FA and AS-C powder in function of temperature

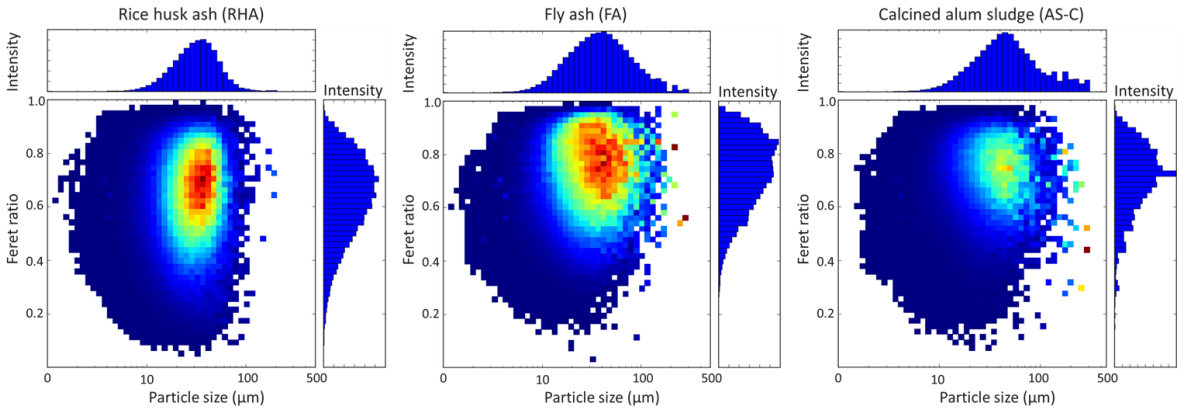

Figure S2: Particle size and shape distribution of the waste powders (RHA, FA and AS-C) in function of volume percentage in the sample.

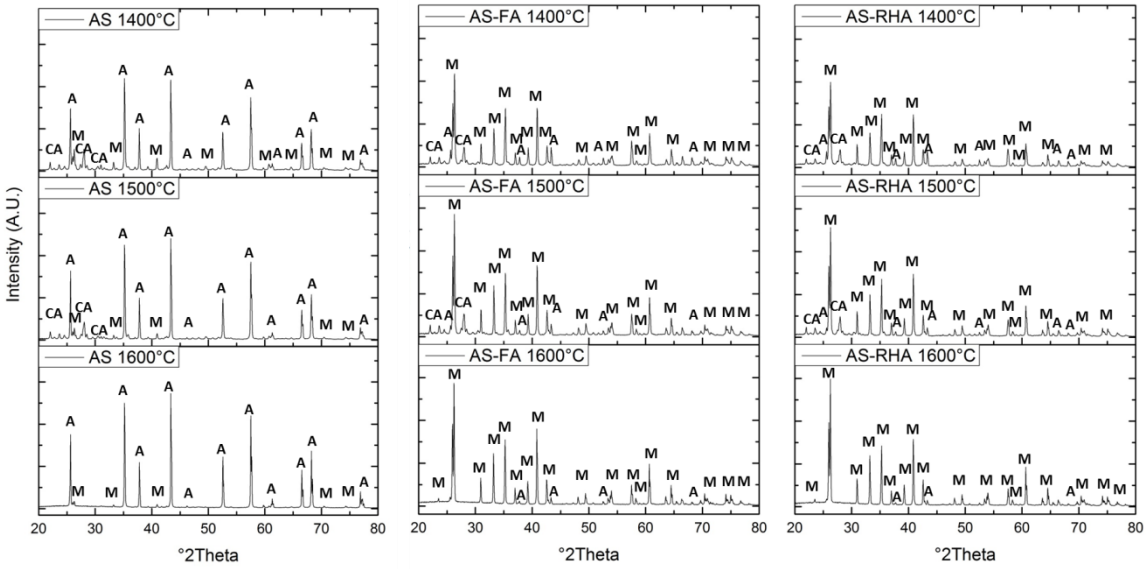

Figure S3: XRD patterns of the AS/M, AS-FA/M and AS-RHA/M microspheres after sintering 1 hour at different temperatures with indication of the crystal phases: α-alumina (A), mullite (M) and calcium aluminum silicate (CA)

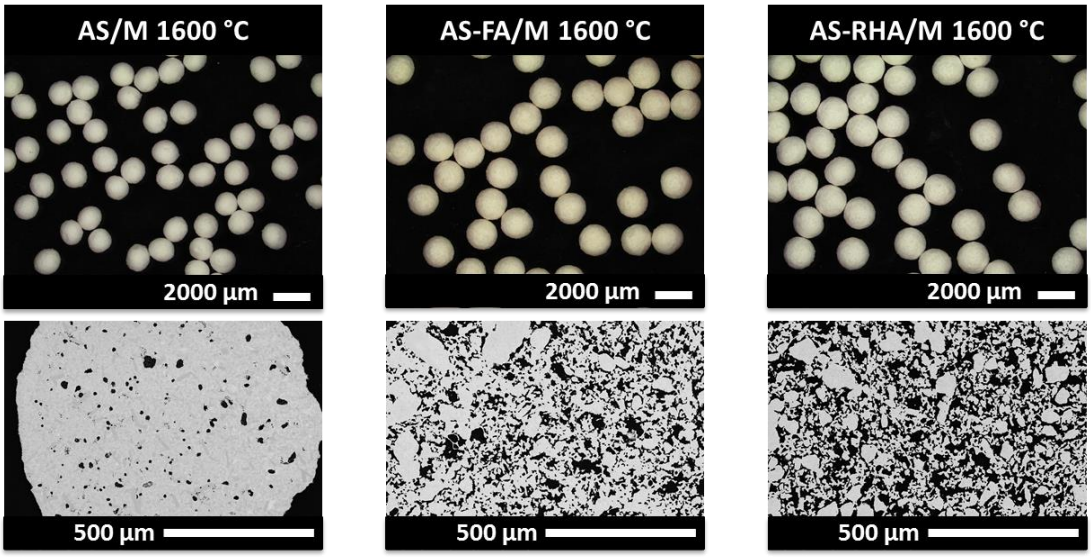

Figure S4: Optical microscopy images of the sintered microspheres (1h at 1600 °C) in correlation to the SEM images on their cross section

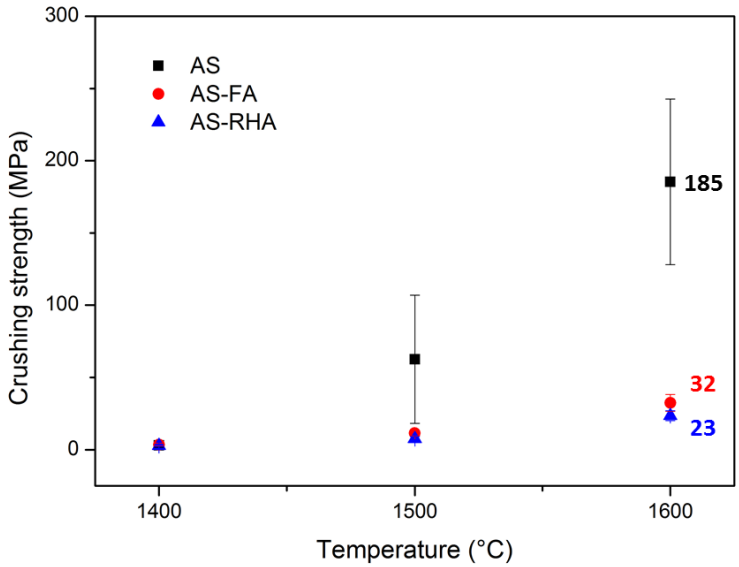

Figure S5: Crushing strength of the microspheres in function of sinter temperature